Modeling of the As (III) adsorption using Fe impregnated polyethylene terephthalate char matrix: A statistical approach

Ghazi Mohd Sawood[a], Shashi Bala Gautam[b], Ashutosh Mishra[a,*], Shobhit Dixit[c] and Neeta Singh[a]

[a] Department of Chemical Engineering, Dr. Ambedkar Institute of Technology for Handicapped, Kanpur 208024, India
[b] Department of Chemical Engineering, Government Polytechnic, Kanpur 208002, India
[c] Department of Chemical Engineering and Technology, IIT BHU, Varanasi, Uttar Pradesh, 221005, India
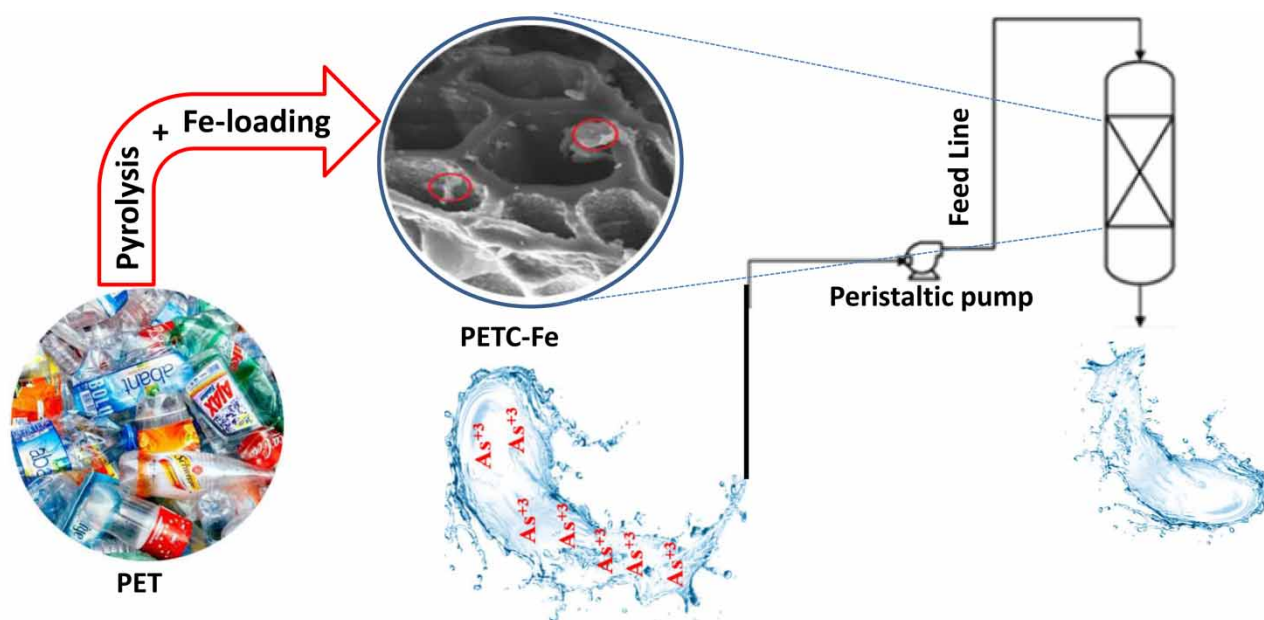*Corresponding author. E-mail: ashutosh@aith.ac.in

ABSTRACT

The present research aimed to analyse the impact of economical Fe impregnated polyethylene terephthalate (PET) char (PETC-Fe) for adsorption of As (III) through series of column experiments. For an inlet arsenite concentration of 1,000 μg/L, PETC-Fe exhibits excellent uptake capacity of 1,892 μg/g. Central composite design (CCD) in response surface methodology (RSM) was used to evaluate the influence of various process variables on the response function (breakthrough time) for optimization and assessment of interaction effects. The breakthrough time is more responsive to influent As (III) concentration and bed height than inlet flow rate, according to the perturbation plot. Adams–Bohart, Bed Depth Service Time (BDST) model, and Thomas models were used to model the dynamics of the adsorption system. The BDST model suited the experimental data well in the early part of the breakthrough curve, but there were minor variations over the break-points. Despite the fact that the experimental values and the data sets estimated using the Adams–Bohart model followed a similar pattern, they differed slightly. The PETC-Fe was found to be a sustainable and highly economical adsorbent, with a desorption performance of more than 97%, indicating the adsorbent's reusability. This adsorbent's excellent As (III) uptake capacity and regeneration performance imply that it might be used in industrial/domestic applications, and the information obtained could aid in future scaling up of the adsorption system.

Key words: adsorption, central composite design, PET, PETC-Fe adsorbent, RSM
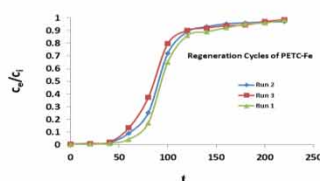
HIGHLIGHTS

- Fe loaded PET char is a viable alternate adsorbent for the adsorption of As (III).
- PETC-Fe exhibits excellent uptake capacity of 1,892 μg/g.
- The breakthrough time is more responsive to influent As (III) concentration and bed height than inlet flow rate.
- The BDST model suited the experimental data well.
- The regeneration and persistence of the PETC-Fe in subsequent cycles were also justified.
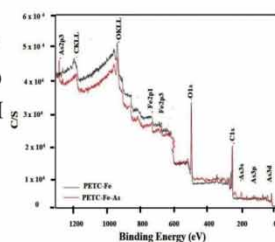
GRAPHICAL ABSTRACT
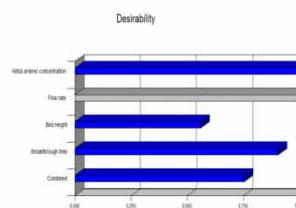
INTRODUCTION

Arsenic (As) has become a major environmental pollutant across the globe. The most common inorganic arsenic sources in the aquatic system include erosion of arsenic laden minerals, industrial effluent, weed control, and drugs (Singh *et al.* 2022). In water bodies, inorganic arsenic is extensively dissolved and mobilised, and its behaviour is influenced by redox state and pH (Sawood & Gupta 2018). As (III) and arsenate As (V) are the two most common inorganic arsenic forms present in groundwater and industrial effluent. It has a pH range of neutral to slightly acidic or alkaline (Weerasundara *et al.* 2021). It's been proven that arsenic species are hazardous, with arsenite having a greater negative impact on human health than arsenate (Lee *et al.* 2022). Arsenic groundwater pollution is a potential issue around the globe due to its high prospective toxicity and carcinogen nature. As a result, the World Health Organisation establishes a maximum permissible arsenic concentration of 10 ppb for potable water as a normative standard (Dettori *et al.* 2022).

Purification/desalination of potable aquatic system, and facilities related to treatment of waste water, particularly in poor nations, must be modified immediately to address this complex situation (Palansooriya *et al.* 2020). Highly effective and economic techniques for mitigating arsenic from aquatic aquifers are highly suggested for this application. Numerous methods for mitigation arsenic from the aquatic system have been developed over the last few decades, comprising oxidation, coagulation/flocculation, filtration, precipitation, and adsorption, ion exchange, and membrane separation (Pal *et al.* 2021). Because of its lower cost, ease of operation, and low disposal of wastes, adsorption is one of the most effective methods among them

(Sawood & Gupta 2020a). Despite several shortcomings such as hydrophilic nature and blocking of pore, carbon based adsorbents have been considered a suitable strong material owing to their relatively low cost.

Due to the obvious constraints of the existing adsorbents, it was suggested that plastic generated chars can be used for contemporaneous arsenic adsorption. Amongst all the other solid wastes produced, plastics have proven to be a devastating concern to control and eradicate from the ecosystem (Foglia 2021). The expanding consumption of plastics has resulted in an annual increase in waste generation. Considering the fact that a large portion of plastic trash is repurposed and energy is recovered, some of it will undoubtedly be buried in landfills, polluting aquifers and emitting ozone-depleting chemicals into the air. As a result, it is not an adequate method for dealing with these contaminants (Hopewell et al. 2009). Furthermore, the scarcity of available land for dumping plastic garbage, as well as its harmful repercussions, necessitates the development of an additional strategy for managing waste material. As a result, the current study proposed an efficient approach for controlling and redirecting them from landfills for use as superior arsenic sorption. An approach for recycling polyethylene terephthalate (PET) trash by processing it into cross-linked hydrogels by PET aminolysis has been suggested. When evaluated as sorbent materials for an anionic dye like Congo Red, PET-derived hydrogels rich in amino groups and aromatic compounds were reported to have a 500 mg/g dye uptake capacity (Chan & Zinchenko 2021). The extraction of EBT dye from secondary effluent has been made possible by the development of metal-organic framework adsorbent from recycled PET bottles. The developed PET-derived MOF is characterized as a credible, added-value substance that serves as a long-lasting adsorbent for organic dyes observed in wastewater (Bool et al. 2022). In terms of uptake rate and capacity, the PET-based activated carbon display superior adsorption behaviour toward p-nitrophenol compared to commercial activated carbon (Mendoza-Carrasco et al. 2016).

The majority of the published research on arsenic removal by adsorption focuses on arsenate with only a few investigations on arsenite mitigation in fixed bed columns (Maia et al. 2021; Razzak et al. 2021). Researchers developed a variety of adsorbents for the removal of arsenite from aqueous system, with varying degrees of effectiveness. Arsenite mitigation by coconut husk char (Yeo et al. 2021), manganese oxide/sand matrix (Bajpai & Chaudhuri 1999), basic $C_3O_9Y_2$ (Wasay et al. 1996), and granules of TiO_2 (Bang et al. 2005). Metal oxides, such as ferric ox-hydroxide, Al_2O_3, and MnO_x, have proven to have excellent arsenic uptake capacities on their respective surfaces. Because of their higher affinity for inorganic arsenic compounds, ferric ox-hydroxide is extensively used as adsorbent materials. Adsorption of arsenate and arsenite by ferric ox-hydroxide has been reported (Goldberg 2002). They observed that these materials are more effective in mitigating arsenite then adsorbing arsenate in natural aquatic system. Manganese oxides have gained wide acceptance as oxidizers for the adsorption of arsenite (Islam et al. 2018). Mn (4+) is converted to Mn (3+), which is then reduced to Mn (2+) in the entire oxidation-reduction reaction process. Natural Fe_2O_3 as well as Fe-abundunt soil (lateritic) have been found to be effective in adsorbing As (III) from aqueous solution. These minerals are available in large quantities and considerably cheaper (Aredes et al. 2013). The uptake of aqueous arsenic was enhanced in Fe-loaded biochar ($q_{max} = 2,160$ µg/g), which was prepared by stirring a solution of Fe salt with biochar. The resulting matrix, on the other hand, has very little magnetization, making it difficult to collect after sorption for regeneration (He et al. 2018). Nevertheless, the majority of As (III) removal investigations have been carried in batch mode, but every adsorbent has advantages and disadvantages with respect of reuse and regeneration, material strength, uptake capacity, pressure drop through fixed bed runs, and so on. Batch reactors are simple to use in a lab setup, but they are impractical in the field operations. Furthermore, because precise scale-up results for column arrangements cannot be acquired from batch findings, the adsorbent's real time applicability should be determined in fixed bed column experiments. There are distinct advantages of adsorption on columns operations. It's easy to use, produces large yields, and can simply be scaled up from a lab setting.

The current research focused on the utilisation of plastic carbon based, Fe loaded matrix as a cost-effective material for As (III) removal, as determined by mild carbonization of plastic trash. Even in extremely small concentration, it is reported to have devastating effects on the human health and environment. Although a variety of adsorbents have been employed to reduce As (III) from polluted areas, the application of chars derived from such waste plastics (PET) is a novel subject of concern. Because of As (III) affinity for Fe, a complex material (Fe_2O_3-imprignated PET char (PETC-FE)) was employed as an adsorbent to investigate its column effectiveness for As(III) removal under up flow circumstances in a column mode after encouraging findings in batch experiments. Breakthrough experiments were conducted to determine the influence of process parameters (influent flow rate, bed height, and inlet concentration) on the breakthrough curve. The adsorption tests were quantitatively modelled employing central composite design (CCD) for sensitivity studies and optimization capacities. Individuals and the cumulative influence of various variables influencing the adsorption mechanism have been studied using the

model. Various kinetic models, such as BDST model, Thomas model, and Adam-Bohrat model, were used to simulate the dynamics characteristics of the adsorption. Furthermore, this would be a major boon because it would address both the challenges of waste disposal and heavy metal adsorption utilising a previously existent resource. These can be efficiently used on practical application for the treatment of other heavy metals based on the conclusions gained from examining the prevalent processes and sorption performance of the PET char.

A comprehensive study has been conducted to find an affordable, simple, and environmentally sustainable resolution to disastrous As (III) contamination that may be adopted in poor countries. The findings of this research are presented and discussed.

MATERIALS AND METHODS

Materials

All the used chemicals were of reagent grade. The sample containers and glassware were cleansed with a soap solution followed by washing using tap water. They were soaked for a minimum 24 h in 15% HNO_3, and then rinsed thrice with deionised water. The aqueous solutions used were prepared with distilled water. As (III) stock solutions were prepared with As_2O_3 (arsenic trioxide) and NaOH, both procured from Merck. 1.3 g of arsenic trioxide As_2O_3 was dissolved in a minimum amount of 20% sodium hydroxide to make As (III) standard solution. It was then diluted to 1 L after being neutralised with HNO_3 (Giri 2019).

Synthesis of modified plastic char

Waste PET (polyethylene terephthalate) has been used as a precursor to synthesise plastic chars. Pyrolysis has been done to transform the materials into plastic char after they were prepared with feedstock. Pyrolysis was conducted in a lab scale arrangement consisting of specimen holder, condenser, fluid collectors, muffle furnace, flow meter. In every test run, sample (100 g) was loaded in the reaction zone of muffle furnace and heated to obtain the char. Pyrolysis was carried out under inert conditions at temperatures of 500, 600, and 700 °C, with an 10 °C/min heating rate. Subsequently, the synthesised chars were sieved to get material having particle size in 400–800 μm range. In an Erlenmeyer flask, 10 g PETC was stirred with 1 L 0.1 M $FeCl_2$ procured from Merck India, with adjusted pH between 3 and 5 (Asghar *et al.* 2015). The flask was then stirred for a day at 25 °C temperature in a shaker at 70 rpm. The extract was then filtered and the remnant was rinsed numerous times with double distilled water to remove any metal salts and residual precipitates attached to the exterior surface of the PETC-Fe material.

Analytical procedure and characterization

The characterization of synthesized PETC-Fe was done for analysing decomposition characteristics, ultimate and proximate analysis, etc. A thermo-gravimetric analyser (STA 8000 Perkin Elmer) was used to perform thermogravimetric analysis (TGA) on the prepared adsorbent. The CHN/O elemental analyser was being used to examine the elemental compositions. The structural properties of PETC-Fe were carried out using D8 Focus X-Ray diffraction (XRD) equipment. Energy dispersive X-ray diffraction (EDX) coupled scanning electron microscopy (SEM) (Carl Zeiss model-EVO-50) was used to examine the morphology PETC-Fe. A Stenner-85 peristaltic pump was employed to provide a constant supply of As (III) solution to the fixed bed column. An inductively coupled plasma mass spectrometry (ICPMS) (Agilent-7900) was used to measure As (III) from the test solution, and a pH meter was used to measure the pH of the solution (model Hanna-HI2020). MEXA-6000FT model Fourier transform infrared (FTIR) were used to investigate the functional groups present in the adsorbent.

Experimental setup

Fixed-bed column experiments were performed utilizing 2 cm internal diameter and 60 cm long borosilicate glass columns. For the purpose of produce varying bed heights, the column was loaded with various amounts of PETC-Fe within two fixed glass wool (0.5 cm) layers. The supporting layers of glass wool were provided to avoid the floatage of PETC-Fe. Using central composite design in response surface methodology (RSM), a column analysis was carried to investigate the impacts of operational variables (influent As (III) concentration, bed height, and influent flow rate on the response function (breakthrough time) of As (III) adsorption. As (III) solutions with the required influent concentration were regulated to the appropriate pH for maximum As (III) uptake and injected into the column in down-flow mode at the specified flow rate through the bed. The

flow rates were selected to provide enough runoff per 45 min to allow for realistic analysis of arsenic levels. When the effluent As (III) concentration surpassed 99% of the influent concentration, the column's operation was halted. All tests were carried out in triplicate at room temperature with a 3% experimental error limit and mean results reported.

Breakthrough curves modeling

The breakthrough curve's shape generated from plotting C_f/C_i against time t, where C_f and C_i is the outlet As (III) and influent concentrations in µg/L, respectively, can be used to evaluate the efficiency of a column. This is necessary to ascertain a fixed bed column's operation and dynamic responsiveness (Chowdhury *et al.* 2015). For a given influent flow rate and inlet concentration, the mass of As (III) adsorbed by PETC-Fe in the fixed bed, viz $q_{overall}$ (µg), is equivalent to the area underneath the curve of the removed adsorbate concentration, C_a $(C_i - C_f)$ (µg/L) against t (min), and is represented by equation:

$$q_{overall} = \frac{Q}{1000} \int_0^t dt \tag{1}$$

where Q represents flow rate (volumetric) and t is flow time (min).

Equation (2) is used to compute the experimental adsorption capacity, q_e (µg/g), where W is the overall dry mass of As (III) in the bed (g)

$$q_e = \frac{q_{overall}}{W} \tag{2}$$

Equation (3) is used to calculate the total quantity of As (III) loaded into the fixed bed column (mg)

$$W_{overall} = \frac{c_f Q t}{1000} \tag{3}$$

BDST, Thomas, and Adams–Bohart are mathematical models used to examine the breakthrough curves, in the present study.

Adams–Bohart model

According to the Adams–Bohart model, rate of adsorption is proportional to both the concentration of the adsorbate and the adsorbent's leftover capacity. The first half of the breakthrough curve is described using Adams–Bohart model (Burdzy *et al.* 2022).

$$\ln\left(\frac{C_f}{C_i}\right) = KC_i t - KN_0 \frac{h}{U} \tag{4}$$

where k represents constant of kinetic (L/µg-min), u is the linear velocity determined by taking ratio of the volumetric flow rate and column's area, h is the bed height (cm) of column, and N_o is the maximum uptake capacity (µg/L). A graph of ln (C_f/C_i) against t can be used to determine the values of constant of kinetic and N_o.

The Thomas model

The Thomas model assumes the operation is based on Langmuir model without any axial mixing in column uptake, as the deriving force for rate is based on second-order kinetics of reaction. The Thomas model in linear form can be represented as follows:

$$\ln\left(\frac{c_i}{c_t}\right) - 1 = k_{th} q_0 \frac{m}{Q} - k_{th} C_0 t \tag{5}$$

where k_{th} represents model constant (mL/min-µg), q_0 is the uptake capacity (µg/q) of adsorbent at equilibrium, m represents mass (g) of PETC-Fe, and Q represents volumetric flow rate.

BDST model

In fixed-bed column study, the BDST is a straightforward semi-empirical model that allows for the quickest forecast of adsorbent efficiency. The BDST model assumes that adsorption rate is governed by the strong interaction between the As (III) and the PETC-Fe's non-utilized capacity (Igwegbe *et al.* 2021). This model can forecast the link between the fixed bed column's bed height and service time. The below mentioned equation gives a linearized relation between bed height and service time.

$$t = \frac{N_0 Z}{U C_i} - \frac{1}{K C_i} \ln\left(\frac{C_i}{C_f} - 1\right) \tag{6}$$

where k represents the BDST model's rate constant (L/mg-min), N_0 represents the (μg/L), and Z denotes the height of the packed bed (cm).

Design of experimental and optimization by RSM-CCD

RSM is a technique which can be used to model experimental procedures. This process relies on quantitative regression model, which includes finding an optimum model to minimize remaining variances. RSM was originally designed to identify the optimal process variables in the process industry, but it is today employed in a wide range of domains and applications, including not just physical sciences and engineering, but also physiological, medical, and sociology fields (Dixit & Yadav 2019). Presently, a quantitative optimization model has been designed using the RSM based on the (Design-Expert 6.0.8 software) for investigating the combined impact of the process variables (influent As (III) concentration, bed height and flow rate) on the response function (breakthrough time). The statistical model is generated using the CCD programme in terms of uptake of As (III), as it uses the smallest number of samples necessary to optimise the observed process parameters while obtaining the highest breakthrough time.

RESULTS AND DISCUSSION

TGA was used to examine the decomposition characteristics of the raw PET. The ultimate, proximate, and Brunauer-Emmett-Teller (BET) analyses of the synthesised PET chars were also used for detailed characterization (Table 1). Furthermore, the dominant processes and the adsorption effectiveness of the investigated PETC-Fe were investigated. In the following sections, the outcomes of all of these have been reported and discussed.

The moisture content of the PET sample was reported as 1.98 in proximate analysis. Pyrolysis of PET yielded 85.6% volatile matter, suggesting that solid compounds such as ash content and fixed are formed less frequently. The specimen had no N but high C content, according to elemental analyses. PETC had fewer amounts of fixed carbon, 9.31%, but the high amount of C, 71.4%, indicating that while the degree of char produced will be smaller, but the quality will be superior due to the high C content.

SEM imaging is used to analyse the surface morphological properties of the PETC and PETC-Fe (Figure 1(a) and 1(b)). After modification, the PET surface is relatively smooth, however, considerable number of pores and heterogeneity is visible in PETC, indicating that it possesses high porosity, which may have resulted in a huge surface area. PETC-Fe surface is coated by numerous particles, indicating a coating of Fe_2O_3 molecules bonded to the PETC surface. The BET pore size, and pore volume of PETC-Fe are shown in Table 1. After Fe loading, the BET parameters corresponding to PETC-Fe reduces. This reduction could be attributed to pore occlusion caused by Fe coating in the PETC samples. Due to iron doping, a similar trend of reduction in BET parameters has previously been observed in literature (Sawood *et al.* 2021a). PETC-Fe has an average pore size of 5–15 Å, indicating that it is microporous in nature.

Table 1 | PA, UA and BET analysis results

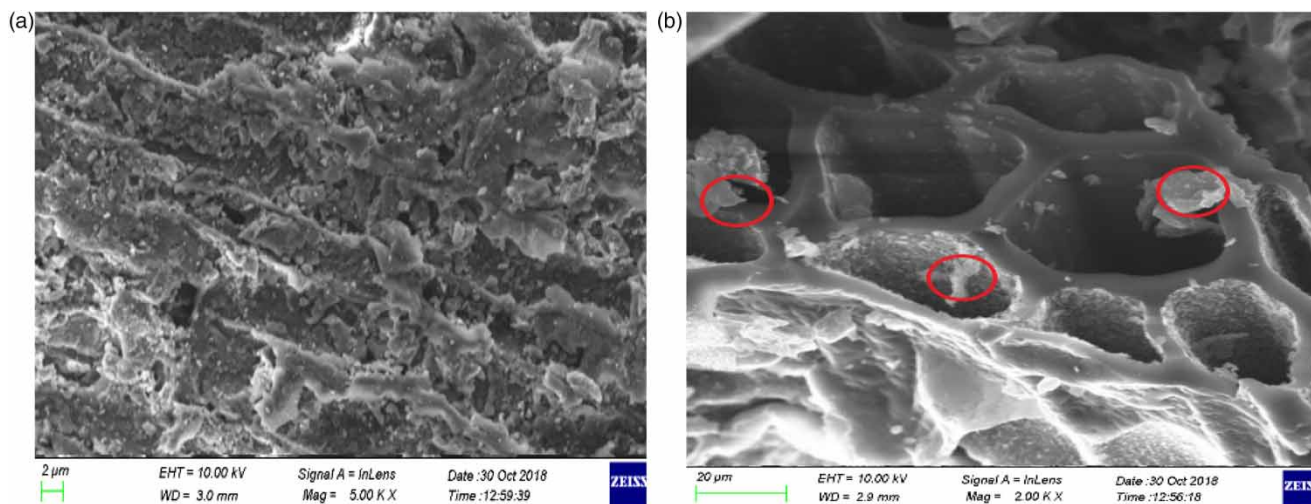| Proximate analysis		Ultimate analysis		BET analyses		PETC	PETC-F
Moisture content	1.98	Carbon (C)	71.4			PETC	PETC-F
Fixed carbon	9.31	Oxygen (O)	23.8	Surface area (S_{BET}) (m²/g)		81.4	33.6
Volatile matter	85.6	Hydrogen(H)	4.3	Pore size (Å)		4.73	3.55
Ash content	6.14	Sulphur(S)	0.5	Pore volume (cc/g)		3.94	3.12

Figure 1 | SEM micrographs of PET (a) PET precursor and (b) PETC-Fe.

Figure 2 demonstrates the X-ray diffraction analysis (XRD) findings of PETC and PETC-Fe. Two diffraction crests at 27.42° and 60.12° have been allotted to the IP 118 and 626 of silicon dioxide a diffraction peak at 39.38° and 68.92° to the indexed planes 109 and 7-4-2 of Ca_2O_4Si, and a diffraction peak at 49.78° to the IP (128) represents $CaCO_3$. Fe was considered to be present on the surface of PETC-Fe, as reflected by Fe_2O_3, γ-Fe_2O_3 (36.8° and 65.6°) and Fe_2O_3 (34.23° and 41.52°) peaks (PDF42-0718) (Gong *et al.* 2016). It's noteworthy that silicon dioxide, Ca_2O_4Si, and $CaCO_3$ seem to be non-visible in the X-ray diffraction pattern of PETC-Fe, which could be due to the lower concentration of these constituents after Fe was impregnated. Fe_2O_3/silica was claimed to have the potential to extract aqueous As (III) (Tajik *et al.* 2021). The increase in uptake of adsorbate owing to Fe inoculation outweighed the decrease in uptake due to the loss of silicon dioxide, Ca_2O_4Si, and $CaCO_3$ in this study.

Figure 3 depicts the variations in FTIR analysis of the PETC, PETC-Fe, and PETC-Fe-As composites. At wavelengths of 1,578, 1,390, 876, and 864 cm^{-1}, four peaks were observed for PETC, that were attributed to the vibrations of the carbonyl, cyclic esters, aromatic H_2, and C, respectively (Ahmed *et al.* 2016). Five peaks were identified with PETC-Fe: 3,300 cm^{-1} (hydroxyl), 1,578 cm^{-1} (carbonyl), 1,390 cm^{-1} (cyclic esters), 876 cm^{-1} (aromatic H_2), and 864 cm^{-1} (methyl). For PETC-Fe, a new peak was found at 3,300 cm^{-1}, probably corresponded to hydroxyl. In addition, the carbonyl
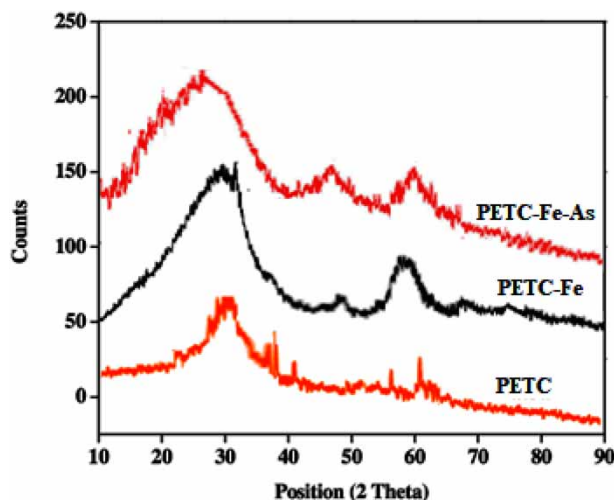

Figure 2 | XRD patterns of PETC (lowermost), PETC-Fe (middle), PETC-Fe-As (upmost).
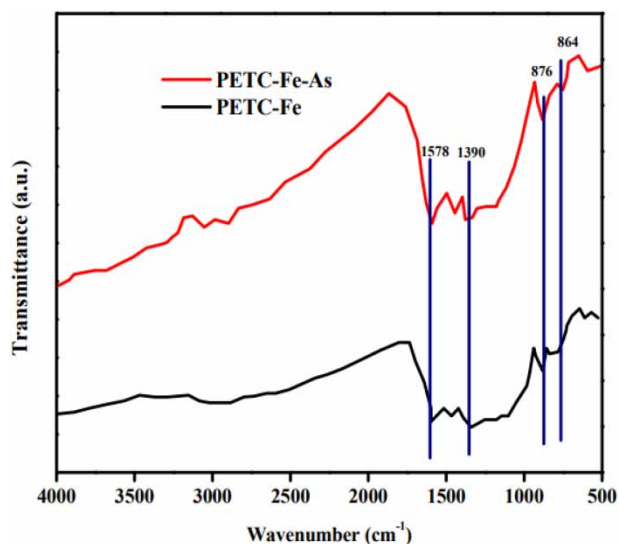
Figure 3 | FTIR spectra of PETC-Fe and PETC-Fe-As.

$(1,576 \text{ cm}^{-1})$ intensity increased (Tang *et al.* 2016). More O_2 laden groups (hydroxyl and carbonyl) were detected for PETC-Fe, implying that iron loading affected the functional groups on the exterior of the PETC.

The PETC-Fe exhibited ferromagnetic characteristics having significant magnetization (saturation) and was rapidly recollected by a magnetic force; however, the PETC exhibited no sensitivity and distributed well in the solution. The PETC-Fe was still usually attracted by a magnet after a week of stirring at room temperature and 90 rpm. These results indicated that the magnetic properties were present in the PETC-Fe. The magnetic behaviour of PETC-Fe was determined using a VSM at 25 °C temperature, as illustrated in Figure 4. The PETC-Fe exhibits ferromagnetic characteristics at 298 K, with a saturation magnetization (SM) of 68.4 emu/g. The theoretical SM of bulk – iron (III) oxide (76 emu/g) was comparable to this value.

Binding energy modifications for Fe, As, C, and O were discovered using XPS analysis to further elucidate the mechanisms of As (III) uptake PETC-Fe. Figure 5 demonstrates that the outer layer of precursor is solely dominated by C, O groups, whereas Fe, and As emerged in PETC-Fe after Fe impregnation and adsorption, respectively. Both pre- and post-As (III) sorption, two distinct Fe peaks related to Fe2p3, and Fe2p1 were detected on the surface of PETC-Fe. After adsorption of As (III),
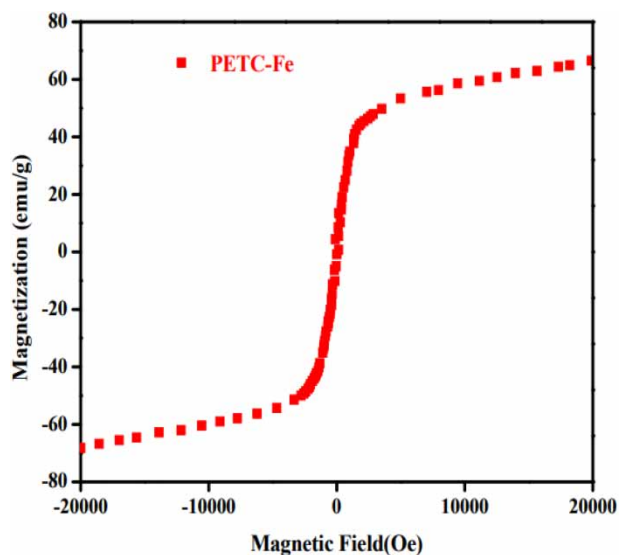

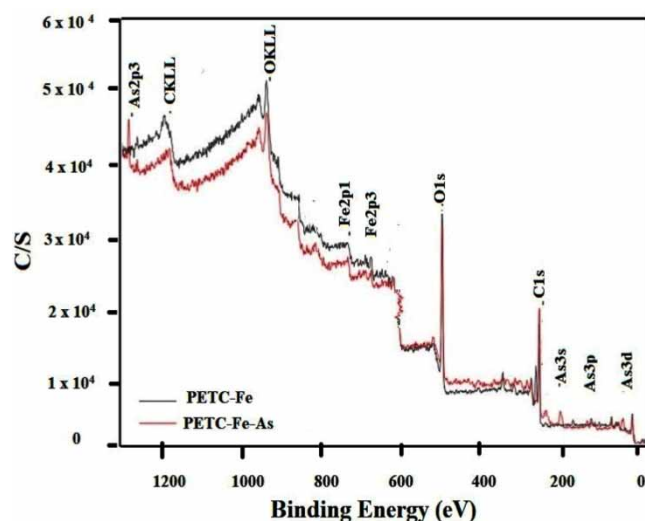**Figure 4** | Magnetization plot of PETC-Fe.

Figure 5 | The XPS spectra of PETC-Fe before and after As(III) adsorption.

a noticeable peak related to As3d was observed on the surface of PETC-Fe. After Fe loading, the atomic % of C dropped significantly, whereas that of O increased substantially. The O/C atomic ratios pre- and post-As (III) uptake were reported as 0.91 and 0.64 for PETC-Fe and 0.18 for precursor, respectively. This explains that after Fe loading, the O functional groups enhanced, but after As (III) adsorption, they reduced.

Response surface methodology for optimization:

RSM has become extremely prevalent for designing, enhancing, and optimising complicated processes, as well as determining the significance of different operating variables (Mondal *et al.* 2019). For a set of three independent variables, namely, influent As (III) concentration, inlet flow rate, and bed depth, the most efficient CCD in RSM was employed to study their effects on the breakthrough time for fixed-bed continuous of As (III) by PETC-Fe. Table 2 lists the variables' testing limits, as well as their notation and unit in central composite design.

With the help of the Design Expert (6.0.8), a 2^3 complete factorial central composite design was obtained. A total of 20 tests in duplicate were used to the central composite design matrix according to this approach, as shown in Table 3.

ANOVA and model assessment

Analysis of variance (ANOVA) can be used to further examine the model's feasibility and validity (Tables 4 & 5). F-value (Fisher variation ratio), lack of fit, *p*-value (probability value), adequate precision (AP), R_d^2 (coefficient of determination), R_{Adj}^2 (adjusted coefficient of determination), R_{Pred}^2, were some of the evidences. AP corresponds to signal to noise ratio, which predicts contrasts, the range of expected values at nodes to the prediction error. Model selectivity is adequate when the ratios are higher than four (Zhou *et al.* 2011; Mishra *et al.* 2021; Sawood *et al.* 2021b).

The preferred quadratic method was verified using ANOVA, which revealed high Fisher variation ratio value, extremely low probability value (<0.0001), not significant lack of fit value, and coefficient of determination, R_{Pred}^2, and AP. Furthermore, Figure 6 displays the actual vs expected values of As (III) uptake for the continuous column investigation, revealing that the predicted and actual values are in great agreement.

Table 2 | Testing levels and ranges of operational parameters

Factor	Name	Units	Minimum	Maximum	Coded low	Coded high
A	Influent As(III) concentration	μg/L	300.00	1,500.00	$-1 \leftrightarrow 300.00$	$+1 \leftrightarrow 1,500.00$
B	Influent flow rate	mL/min	3.00	9.00	$-1 \leftrightarrow 3.00$	$+1 \leftrightarrow 9.00$
C	Bed height	cm	5.00	15.00	$-1 \leftrightarrow 5.00$	$+1 \leftrightarrow 15.00$

Table 3 | CCD for independent operational variables and the recorded response for As (III)

| | | Factor 1 | Factor 2 | Factor 3 | Response breakthrough time | |
| | | | | | Experimental values | RSM predicted |
Std	Run	A: Influent As(III) concentration µg/L	B: Influent flow rate mL/min	C: Bed depth cm	min	
10	1	1500.00	6.00	10.00	412	417
7	2	300.00	9.00	15.00	858	861
9	3	109.08	6.00	10.00	496	501
4	4	1500.00	9.00	5.00	232	238
5	5	300.00	3.00	15.00	934	941
16	6	900.00	6.00	10.00	468	463
14	7	900.00	6.00	15.00	778	782
17	8	900.00	6.00	10.00	468	463
18	9	900.00	6.00	10.00	468	463
3	10	300.00	9.00	5.00	281	277
2	11	1500.00	3.00	5.00	298	291
13	12	900.00	6.00	5.00	245	240
8	13	1500.00	9.00	15.00	741	735
6	14	1500.00	3.00	15.00	792	789
11	15	900.00	6.00	10.00	468	463
20	16	900.00	6.00	10.00	468	463
19	17	900.00	6.00	10.00	468	463
12	18	900.00	11.05	10.00	425	419
1	19	300.00	3.00	5.00	312	318
15	20	900.00	6.00	10.00	468	463

The empirical relationship between the breakthrough time and the investigated independent process variables, represented in terms of dimensionless regression coefficient by the chosen model, is as follows:

$$\text{Breakthrough time} = +461.57 - 38.72*A - 31.57*B + 273.56*C + 2.46*A2 + 11.9*B2 + 74.39*C2 - 1.31*A*B - 24.54*A*C - 3.84*B*C$$

where A (influent As (III) concentration), B (influent flow rate), and C (bed height) are factors in code.

Table 4 | Sum of squares sequential model

Source	Sum of squares	DF	Mean square	F value	Prob > F	
Mean	5.091E + 006	1	5.091E + 006			
Linear	7.755E + 005	3	2.585E + 005	95.91	< 0.0001	
2FI	4,948.30	3	1,649.43	0.56	0.6497	
Quadratic	34,824.08	3	11,608.03	34.63	< 0.0001	Suggested
Cubic	3,352.06	4	838.01	6.366E + 007	< 0.0001	Aliased
Residual	0.000	6	0.000			
Total	5.910E + 006	20	2.955E + 005			

Table 5 | ANOVA for response surface quadratic model

Source	Sum of squares	df	Mean square	F-value	p-value	
Model	8.153E + 005	9	90,587.12	270.24	<0.0001	significant
A-Influent As(V) concentration	15,612.35	1	15,612.35	46.58	< 0.0001	
B-Inlet flow rate	8,273.95	1	8,273.95	24.68	0.0006	
C-Bed height	7.484E + 005	1	7.484E + 005	2,232.51	< 0.0001	
A^2	27.66	1	27.66	0.083	0.7798	
B^2	983.96	1	983.96	2.94	0.1174	
C^2	18,866.96	1	18,866.96	56.28	< 0.0001	
AB	13.78	1	13.78	0.041	0.8434	
AC	4,816.71	1	4,816.71	14.37	0.0035	
BC	117.81	1	117.81	0.35	0.5665	
Residual	3,352.06	10	335.21			
Lack of fit	3,352.06	4	838.01			
Pure error	0.000	6	0.000			
Cor total	8.186E + 005	19				

Variable interaction

Contour plots were used to investigate the interaction between the various independent factors and their effect on the response (Figures 7–9). The contour plot is a 2D representation of the response surface. This study clarifies the impact of factors and their interactions on the response as a function of two variables simultaneously.

The contour plot of Figure 7 shows the synergetic impact of inlet As (III) concentration and influent flow rate on response (breakthrough time). Within the range of observations, the breakthrough time reduces as the inlet As (III) concentration and influent flow rate rise. This can be elucidated by the fact that PETC-Fe have a finite number of active sites that will be occupied by the adsorbate at a particular concentration (Roy *et al.* 2017; Zhu *et al.* 2018). The active sites on the surface of the adsorbent are now more promptly saturated as the influent As (III) concentration rises, reducing breakthrough time. Uptake capacity was also decreased at increased flow rates due to secant As (III) residence time in the fixed bed and solute diffusion into the adsorbent's pores. As a result of leaving the bed before equilibrium has been established, a lesser breakthrough time is obtained (Mohan *et al.* 2017; Sawood & Gupta 2020b).
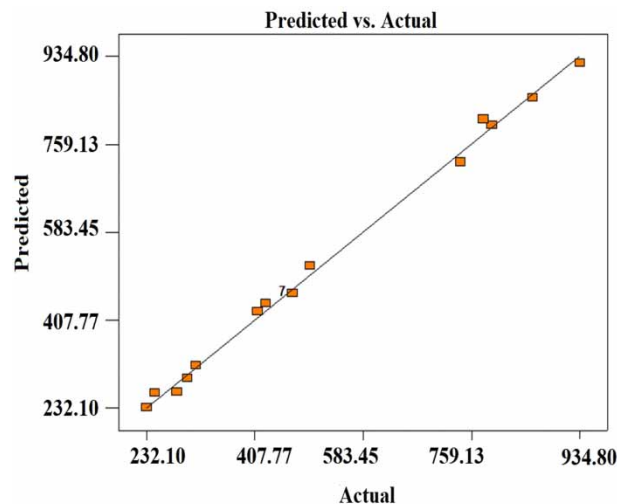
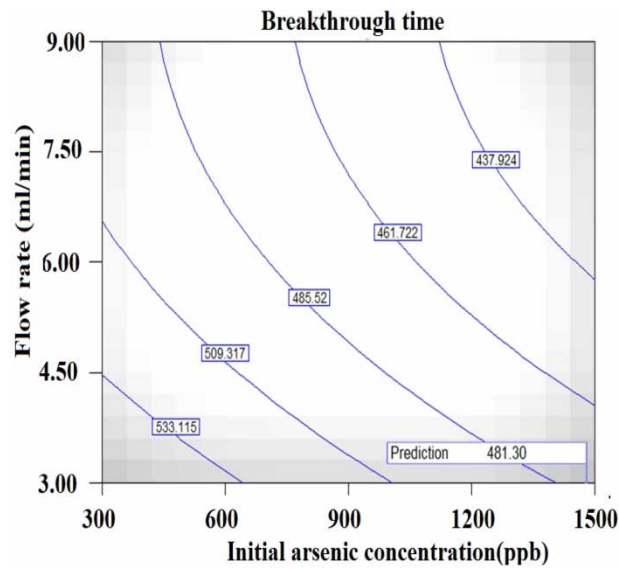**Figure 6** | Predicted vs actual response for fixed bed column operation.

Figure 7 | Contour plot depicting the synergetic impact of influent As (III) concentration and influent flow rate on the response for fixed bed operation of As (III) uptake by PETC-Fe; bed height: 15.0 cm.
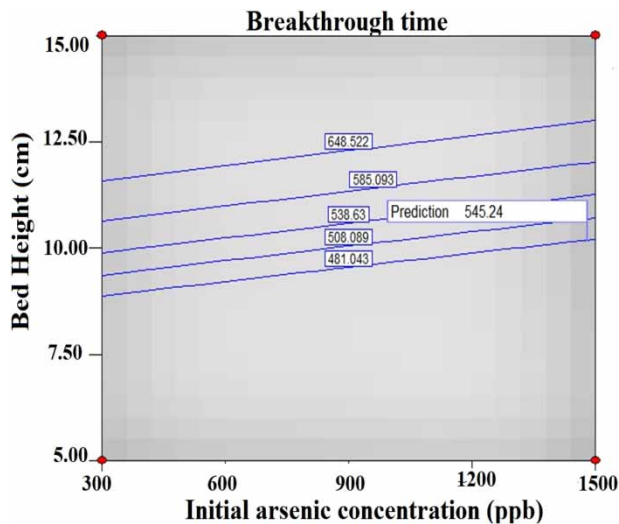

Figure 8 | Contour plot depicting the synergetic impact of bed height and influent As (III) concentration on the response for fixed bed operation of As (III) uptake by PETC-Fe; influent flow rate: 3.0 mL/min.

The interaction impact of influent As (III) concentration and bed height on breakthrough time is displayed in Figure 8. The breakthrough time reduces with increasing influent As (III) concentration and escalates with increasing bed height within the given range of experiment. The obtained pattern could be explained by the fact that enhancement in bed height generates a higher number of available active adsorption sites resulted from enhanced surface area of adsorbent. As a result, the adsorbate has sufficient time to interact with the adsorbent, giving in a prolonged breakthrough (Patel 2020; Yassin et al. 2021).

The synergetic impact of bed height and influent flow rate on the response function for fixed bed column studies of As (III) uptake by Fe–SCC is shown in Figure 9. The breakthrough time is greatly influenced by the interaction between bed height and influent flow rate. The breakthrough time reduces as the influent flow rate increases, but it increases as the bed height increases. As previously stated, such a breakthrough trend can be justified by inadequate residence time of adsorbate in the fixed bed column as well as the presence of active sites.
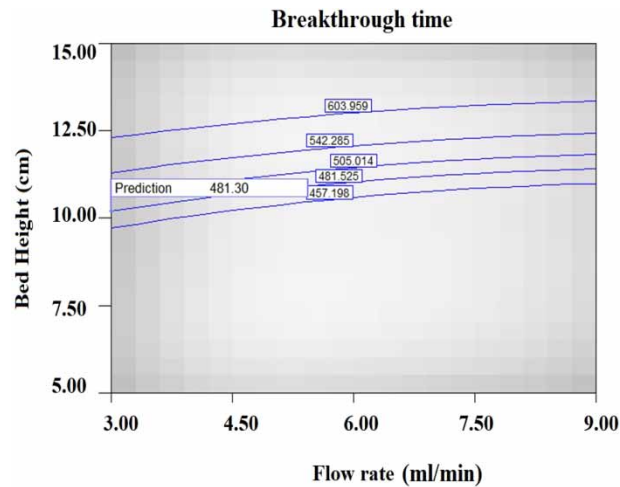
Figure 9 | Contour plot depicting the synergetic impact of bed height and influent flow rate on the response for fixed bed operation of As (III) uptake by PETC-Fe; and influent As (III) concentration: 900.0 μg/L/min.

Thus, contour plots demonstrate that the response function (breakthrough time), increases when concentration of adsorbate reduces, bed height increases, and influent flow rate reduces. At 9.0 cm bed height, 3 mL/min influent flow rate, and 300.0 μg/L adsorbate concentration, the absorption of 1,892 μg/g for arsenic was recorded at the maximum breakthrough time.

According to a survey of the literature, only little works on fixed bed column analysis have been documented; otherwise, the majority of As (III) mitigation research has been undertaken in batch mode. The results collected under batch operations, on the other hand, are often not suitable in real treatment operations, because the residence duration is insufficient to achieve equilibrium. As a result, equilibrium investigations utilising columns are required. Column reactors have a higher equilibrium absorption capacity of As (III), making the adsorbent appealing for As (III) mitigation filter system. Hence, the adsorption capacity of PETC-Fe under fixed bed column operation is contrasted to that of earlier reported different adsorbents (Table 6). Even though it is hard to accurately correlate the PETC-Fe to other adsorbents due to the diverse test conditions

Table 6 | Comparison of the uptake capacities of char based adsorbents for As (III) mitigation by fixed-bed operation

Adsorbent	Operating conditions	Uptake capacity (μg/g)	References
Thioglycolated sugarcane carbon	6.0 g dosage, 3.0 mL/min flow rate, and 1,500 μg/L influent concentration	85.01	Roy et al. (2013)
Iron oxide-coated cement	10–20 cm bed height, 4.3–12 mL/min flow rate and 500–2,700 μg/L initial As(III) concentrations	600.53	Kundu & Gupta (2007)
Multi walled CNTs	10–20 cm bed height, 30.0 mL/min flow rate, and 500 μg/L influent concentration	13.5	Ali (2018)
Fe_2O_3 impregnated aspergillus niger biomass	6.925 g dosage, 2.5 mL/min flow rate, and 100 μg/L influent concentration	88	Pokhrel & Viraraghavan (2008)
Fe_2O_3 nanoneedle array-impregnated biochar fibers	2.0 g dosage, 2,500 breakthrough volume, and 275 μg/L influent concentration	–	Wei et al. (2019)
Non-immobilized sorghum char	150.0 g dosage, 2,500 10.0 mL/min flow rate, and 500 μg/L influent concentration 0.18–1.4 mm particle size	276.5	Carneiro et al. (2021)
Modified calcined bauxite	10 cm bed height, 5.0 mL/min flow rate and 1,000 μg/L initial As(III) concentrations, 0.212 mm particle size	490	Ayoob et al. (2007)
PETC-Fe	15 cm bed height, 3.0 mL/min flow rate	1,892	Current study

used, still the As (III) absorption capacity of PETC-Fe is found to be relatively considerable and comparable to other adsorbents used for As (III) removal in column operations. The findings suggest that PETC-Fe may be efficiently utilised in a continuous fixed bed operations to mitigate As (III) from aquatic environment.

Perturbation analysis

On the response function, the influence of bed height, inlet As (III) concentration and influent flow rate were investigated. A perturbation plot was used to determine the singular impacts of independent process variables viz A (influent As (III) concentration), B (influent flow rate), and C (bed height). The impact of interactions is not used in a perturbation analysis, which is similar to single factor experiments. Figure 10 shows a perturbation plot that may be used to examine the performance of all independent process variables at a certain location in the given design space. Only one factor is altered over the response's range while the remaining factors remain unaltered. A component with a high slope indicates its sensitivity towards the response (Zhang *et al.* 2016). A flattish line indicates that the factor is relatively non-sensitive to variation (Alchouron *et al.* 2020). Breakthrough time (response factor) is highly sensitive towards bed height, influent As (III) concentration rather than influent flow rate, according to the current findings.

Optimization by desirability parameters

Target, minimum, maximum, in range, and set to a precise value are all conceivable goals in the software. The intended aim was favoured for every variable and response in numerical optimization (Amini *et al.* 2008). The desirability analysis of an optimization process are shown in a bar plot (Figure 11) in which the standard was set to max for influent As (III), min for bed height, in range for influent flow rate, and the target was fixed to 'maximum' to analyse commercially sustainable optimum condition. The goal of this procedure was to discover the greatest breakthrough time while operating with the least bed height possible. Independent factors' desirability values range from 0.894 to 1, whereas the aggregate of all variables' desire value is 0.99.

When the independent variables were kept at 10.20 cm bed height, 1,500.0 µg/L of influent As (III) concentrations, and 3.0 mL/min of influent flow rate at a highest desirability point of 0.998, the top maximum response factor (breakthrough time) was found to be 480.58 min.

Finally, identical validation column experiments were carried out under ideal conditions for their confirmation. The experimental test data, which is consistent with the optimised RSM-central composite design result, implies that PETC-Fe could be an effective and cost-effective adsorbent for As (III) mitigation in the aqueous environment.

The optimal parameters for PETC-Fe to adsorb the arsenic were determined and are shown in Table 7.
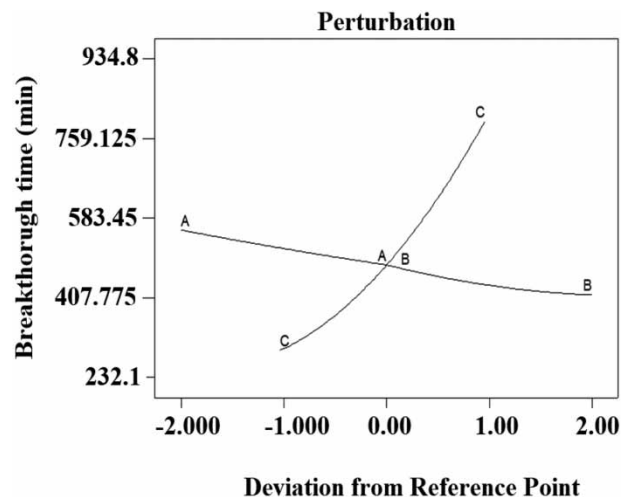

Figure 10 | Perturbation plot depicting the influence of the tested factors on the response is depicted.
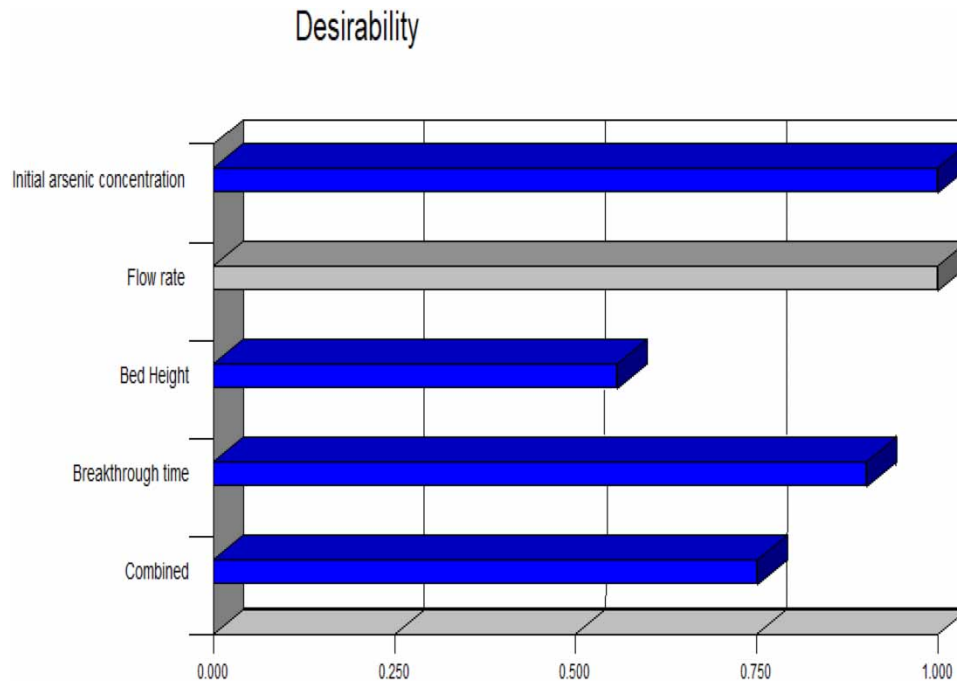
Desirability

Figure 11 | Bar graph representing optimization technique.

Table 7 | Optimum conditions selected for the maximum possible COD removal percentage

Numbers	Influent As(III) concentration	Inlet flow rate	Bed height	Breakthrough time	Desirability
1	300.07	3.00	15.00	941.828	0.993

Modeling of breakthrough curve

Adams–Bohart and Thomas models were utilised to develop a kinetic model in the column and determine the breakthrough curves to explain the fixed-bed column behaviour.

Adams–Bohart model

The Adams–Bohart model for adsorption of As (III) was used to describe the initial section of the breakthrough curve using experimental. The respective values of k_{AB} (kinetic constant) and N_o (maximum uptake capacity) were computed using linear regression analysis on all breakthrough curves and are reported in Table 8. At any flow rates, there is no significant difference

Table 8 | Adams–Bohart parameters at various operating conditions using linear regression analysis

C_i (µg/L)	h (cm)	Q (mL/min)	K	N_o	R^2
300	5	3	0.075	185.22	0.69
300	10	3	0.054	167.83	0.74
300	15	3	0.041	126.53	0.80
300	15	6	0.040	124.71	0.76
300	15	9	0.041	126.42	0.72
900	15	3	0.018	39.44	0.63
1,500	15	3	0.015	37.21	0.61

in the values of the k_{AB} and the N_o. As the bed depth deepens, the values of k_{AB} and N_o reduce. Furthermore, as the initial As (III) concentration rises, the value of k_{AB} falls and N_o rises. The model is described well by theory of surface reaction and posits that equilibrium attainment is not quick; as a result, the rate of uptake is in good accordance with both, the adsorbent's residual capacity and the concentration. Furthermore, the Adams–Bohart model is used in lesser concentration areas and where mass transfer limits the rate of uptake (López-Cervantes et al. 2018). According to Table 8, the actual breakthrough curves are not near to those expected by Adams–Bohart model, and the coefficient of regression (R^2) values are low. As a result, in the range of utilised operating conditions and with present adsorbent, the model cannot be used to predict the experimental findings.

Thomas model

The two unknown variables of the Thomas equation, constant of Thomas model and equilibrium uptake capacity, were determined using the plot ln (Co/Ci 1) against t (linear system form of the Thomas model). Table 3 shows the calculated values of the various parameters of the model, as well as the R^2. According to Table 9, the values of uptake capacity grow as the inlet As (III) concentration and bed height rise, while the values of constant of Thomas model fall, whereas the values of q_o and k_{Th} grew when the flow rate increased. Despite the fact that the Thomas model shows certain reasonable modifications for removal conditions, there is no clear connection in the breaking curve prediction. This can be seen in the disparities among experimental results and model-calculated uptake capacity estimates. Although the Thomas model is among the most frequently used to define the behaviour of biosorption process in column operations, its primary constraint is that it is rooted on second-order kinetics and assumes that biosorption is controlled by interfacial mass transfer rather than the chemical reaction. When this approach is employed to represent biosorption systems under specific circumstances, this mismatch can lead to inaccuracies (López-Cervantes et al. 2018).

BDST model

Plotting the service time t against bed height at Ci/Co equal to 0.15, 0.30, and 0.45 yielded the uptake capacity and rate constant from the BDST model. The tested and expected service times for different bed heights (15, 10, and 6 cm) were estimated using a influent flow rate of 3 mL/min and an influent concentration of 500 μg/L. Table 10 presents the results. The BDST model's projected service time values are consistent with the test service time values. As a result, the BDST model may be suitable for this configuration; also, the significant R^2 values derived from data support the BDST model's applicability for the current fixed-bed column operations.

Table 9 | Thomas model parameters of As (III) uptake on comparison fixed bed column

C_i (μg/L)	h (cm)	Q (ml/min)	K_{th}	q_o	R^2
300	5	3	54.88	896.45	0.71
300	10	3	41.76	1,145.56	0.76
300	15	3	38.50	1,746.20	0.83
300	15	6	44.55	1,971.26	0.74
300	15	9	47.81	2,245.35	0.70
900	15	3	17.45	3,917.52	0.59
1,500	15	3	11.28	6,125.47	0.55

Table 10 | BDST model parameters for As(III) adsorption onto PETC-Fe

c_i/c_e	K	N_o	Service Time (predicted)	Service Time (experimental)	R^2
0.15	844	282.45	346	357	0.989
0.30	21.40	1,541.76	1,341	1,339	0.996
0.45	−9.45	5,985.25	881	817	0.981

Regeneration and reuse

On PETC-Fe, adsorption-desorption experiments cycle for As (III) were performed. The As (III) ions were recovered with 0.050 L of H_3PO_4 (0.1 M). The breakthrough curves for arsenite restoration at 3 mL/min influent flow rate, 15 cm bed height revealed no typical changes through multiple cycles, as illustrated in Figure 12. This shows that PETC-Fe can efficiently withstand repeated use for up to three cycles. For three subsequent sorption/desorption cycles, the regeneration performance was reported to be 99.14, 98.71, and 99.50%, respectively.

The column was cleansed with moderately lukewarm distilled water post-regeneration to clear residual traces of sodium hydroxide and reduce the pH, as adsorption is less effective in the range of basicity. After drying, the column was allowed to operate in subsequent adsorption cycle. Figure 13 depicts three successive sorption cycles, demonstrating that the second cycle's removal effectiveness is reduced by around 8%, followed by depression of another 5% in the third cycle. As can be seen in Figure 13, PETC-Fe offers slightly varying As (III) uptake capacities over the three successive cycles, and the regeneration and reuse of PETC-Fe offers an affordable way to As (III) removal from aqueous system.
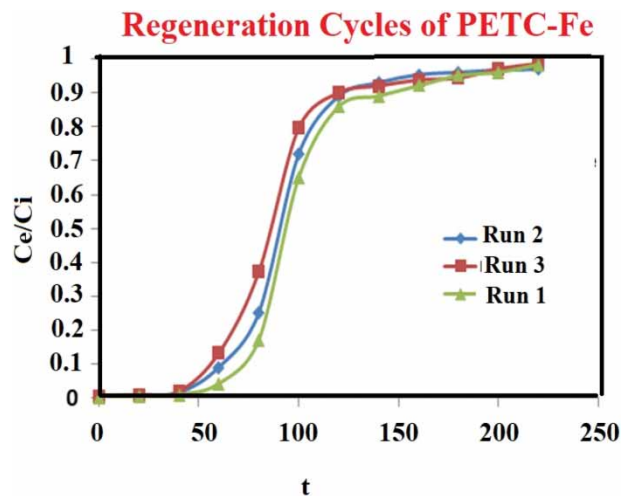

Figure 12 | Effect of consecutive desorption on breakthrough for mitigation of As (III).
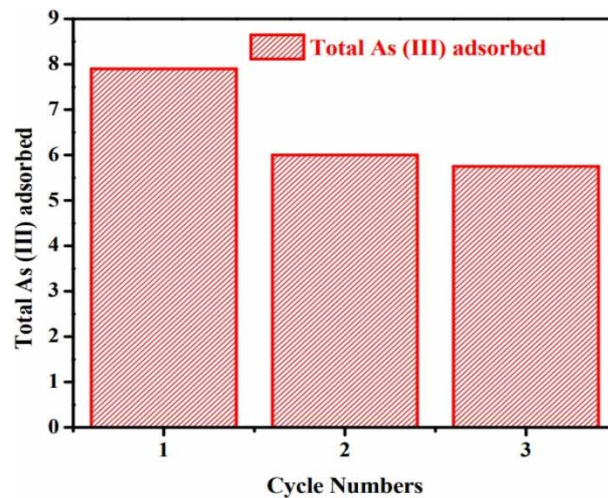

Figure 13 | Capacities of PETC-Fe for As (III) adsorption during three consecutive cycles.

CONCLUSION

Fixed bed column adsorption investigations have been used to evaluate the performance of Fe impregnated chars made from pyrolysis of waste PET for As (III) removal. The impact of independent process variables (bed height, flow rate and concentration) on the breakthrough were designed by CCD. ANOVA confirmed the quadratic model proposed by RSM-CCD. The experimental results were observed to be quite close to the model's predicted values. Contour and perturbation charts were used to predict the impact of the independent variables and their interactions on response function (breakthrough time). The breakthrough time was shown to be highly influenced by the process variables. With a raise in inlet As (III) concentration, the total amount of As (III) adsorbed rose, while the removal percentage reduced. When lesser flow rates and larger bed heights were used, the PETC-Fe column's performance enhanced. Owing to the complicated adsorption mechanism, the BDST approach of breakthrough data estimations slightly differed from the test findings over breakpoint. The results from the column studies did not have a satisfactory correlation with the results from the mass transfer model. According to the optimised CCD result, the PETC-Fe adsorbent has proven to be a sustainable and highly effective adsorbent. Consequently, it can be claimed that use of statistical model is an efficient approach for optimising and design of As (III) removal process. The information reported in this research can be used to design and implement an effective As (III) removal approach even while treating any potable water contamination. For three consecutive adsorption-desorption cycles, the PETC-Fe's regeneration efficiency was observed to be 99.14, 98.71, and 99.50 percent, respectively. This means that the PETC-Fe is capable of being used repeatedly for at least three cycles. The current investigation shows that PET char based adsorbent functions well, indicating that they should be used on a bigger field ranges. As a result, PET char based adsorbent can be regarded as sustainable and novel option for As (III) removal and management of plastic waste.

ACKNOWLEDGEMENTS

DATA AVAILABILITY STATEMENT

All relevant data are included in the paper or its Supplementary Information.

CONFLICT OF INTEREST

The authors declare there is no conflict.

REFERENCES

Ahmed, M. B., Zhou, J. L., Ngo, H. H., Guo, W. & Chen, M. 2016 Progress in the preparation and application of modified biochar for improved contaminant removal from water and wastewater. *Bioresource Technology* **214**, 836–851.

Alchouron, J., Navarathna, C., Chludil, H. D., Dewage, N. B., Perez, F., Pittman Jr, C. U., Vega, A. S. & Mlsna, T. E. 2020 Assessing South American Guadua chacoensis bamboo biochar and Fe_3O_4 nanoparticle dispersed analogues for aqueous arsenic (V) remediation. *Science of The Total Environment* **706**, 135943.

Ali, I. 2018 Microwave assisted economic synthesis of multi walled carbon nanotubes for arsenic species removal in water: batch and column operations. *Journal of Molecular Liquids* **271**, 677–685.

Amini, M., Younesi, H., Bahramifar, N., Lorestani, A. A. Z., Ghorbani, F., Daneshi, A. & Sharifzadeh, M. 2008 Application of response surface methodology for optimization of lead biosorption in an aqueous solution by Aspergillus niger. *Journal of Hazardous Materials* **154** (1–3), 694–702.

Aredes, S., Klein, B. & Pawlik, M. 2013 The removal of arsenic from water using natural iron oxide minerals. *Journal of Cleaner Production* **60**, 71–76.

Asghar, A., Khan, Z., Maqbool, N., Qazi, I. A. & Awan, M. A. 2015 Comparison of adsorption capability of activated carbon and metal doped TiO_2 for geosmin and 2-MIB removal from water. *Journal of Nanomaterials* **2015**, 1–11 .

Ayoob, S., Gupta, A. & Bhakat, P. 2007 Performance evaluation of modified calcined bauxite in the sorptive removal of arsenic (III) from aqueous environment. *Colloids and Surfaces A: Physicochemical and Engineering Aspects* **293** (1–3), 247–254.

Bajpai, S. & Chaudhuri, M. 1999 Removal of arsenic from ground water by manganese dioxide–coated sand. *Journal of Environmental Engineering* **125** (8), 782–784.

Bang, S., Patel, M., Lippincott, L. & Meng, X. 2005 Removal of arsenic from groundwater by granular titanium dioxide adsorbent. *Chemosphere* **60** (3), 389–397.

Bool, R. J. A., Luwalhati, G. C., Tan, N. E. Y., Aquino, A. P. & Maalihan, R. D. 2022 On the use of metal-organic framework-based adsorbent from recycled PET bottles for Eriochrome Black T removal. *Materials Today: Proceedings* **65** (8), 3312–3320.

Burdzy, K., Aurich, A., Hunger, S., Jastrząb, R., Zabiszak, M. & Kołodyńska, D. 2022 Green citric acid in the sorption process of rare earth elements. *Chemical Engineering Journal* **437**, 135366.

Carneiro, M. A., Pintor, A., Boaventura, R. A. & Botelho, C. 2021 Current trends of arsenic adsorption in continuous mode: literature review and future perspectives. *Sustainability* **13** (3), 1186.

Chan, K. & Zinchenko, A. 2021 Conversion of waste bottles' PET to a hydrogel adsorbent via PET aminolysis. *Journal of Environmental Chemical Engineering* **9** (5), 106129.

Chowdhury, Z. Z., Abd Hamid, S. B. & Zain, S. M. 2015 Evaluating design parameters for breakthrough curve analysis and kinetics of fixed bed columns for Cu (II) cations using lignocellulosic wastes. *BioResources* **10** (1), 732–749.

Dettori, M., Arghittu, A., Deiana, G., Castiglia, P. & Azara, A. 2022 The revised European directive 2020/2184 on the quality of water intended for human consumption. A step forward in risk assessment, consumer safety and informative communication. *Environmental Research* **209**, 112773.

Dixit, S. & Yadav, V. L. 2019 Optimization of polyethylene/polypropylene/alkali modified wheat straw composites for packaging application using RSM. *Journal of Cleaner Production* **240**, 118228.

Foglia, A. 2021 *Closing the Plastic Waste Material Cycle in the Power Industry*. University of South-Eastern Norway, Telemark, Norway.

Giri, A. K. 2019 Bioaccumulation potential and toxicity of arsenite using rooted-submerged vallisneria spiralis in a hydroponic culture and its characterization studies. *J. Adv. Sci. Res* **10**, 17–22.

Goldberg, S. 2002 Competitive adsorption of arsenate and arsenite on oxides and clay minerals. *Soil Science Society of America Journal* **66** (2), 413–421.

Gong, Y., Wang, L., Liu, J., Tang, J. & Zhao, D. 2016 Removal of aqueous perfluorooctanoic acid (PFOA) using starch-stabilized magnetite nanoparticles. *Science of the Total Environment* **562**, 191–200.

He, R., Peng, Z., Lyu, H., Huang, H., Nan, Q. & Tang, J. 2018 Synthesis and characterization of an iron-impregnated biochar for aqueous arsenic removal. *Science of the Total Environment* **612**, 1177–1186.

Hopewell, J., Dvorak, R. & Kosior, E. 2009 Plastics recycling: challenges and opportunities. *Philosophical Transactions of the Royal Society B: Biological Sciences* **364** (1526), 2115–2126.

Igwegbe, C. A., Ighalo, J. O., Ghosh, S., Ahmadi, S. & Ugonabo, V. I. 2021 Pistachio (Pistacia vera) waste as adsorbent for wastewater treatment: a review. *Biomass Conversion and Biorefinery* **739** (9), 1–19.

Islam, M. A., Morton, D. W., Johnson, B. B., Mainali, B. & Angove, M. J. 2018 Manganese oxides and their application to metal ion and contaminant removal from wastewater. *Journal of Water Process Engineering* **26**, 264–280.

Kundu, S. & Gupta, A. 2007 As (III) removal from aqueous medium in fixed bed using iron oxide-coated cement (IOCC): experimental and modeling studies. *Chemical Engineering Journal* **129** (1–3), 123–131.

Lee, S. Y., Chang, B., Kim, Y., Jang, H. & Lee, Y. J. 2022 Characterization of arsenite (As (III)) and arsenate (As (V)) sorption on synthetic siderite spherules under anoxic conditions: different sorption behaviors with crystal size and arsenic species. *Journal of Colloid and Interface Science* **613**, 499–514.

López-Cervantes, J., Sánchez-Machado, D. I., Sánchez-Duarte, R. G. & Correa-Murrieta, M. A. 2018 Study of a fixed-bed column in the adsorption of an azo dye from an aqueous medium using a chitosan–glutaraldehyde biosorbent. *Adsorption Science & Technology* **36** (1–2), 215–232.

Maia, L. C., Soares, L. C. & Gurgel, L. V. A. 2021 A review on the use of lignocellulosic materials for arsenic adsorption. *Journal of Environmental Management* **288**, 112397.

Mendoza-Carrasco, R., Cuerda-Correa, E. M., Alexandre-Franco, M. F., Fernández-González, C. & Gómez-Serrano, V. 2016 Preparation of high-quality activated carbon from polyethyleneterephthalate (PET) bottle waste. Its use in the removal of pollutants in aqueous solution. *Journal of Environmental Management* **181**, 522–535.

Mishra, A., Sawood, G. M., Gautam, S. B. & Trivedi, R. K. 2021 Optimization of process inputs for the synthesis of waste rice bran oil isolated Pseudomonas aeruginosa MTCC 424 biosurfactant using response surface methodology for oil recovery applications. *Bioresource Technology Reports* **14**, 100653.

Mohan, S., Singh, D. K., Kumar, V. & Hasan, S. H. 2017 Effective removal of Fluoride ions by rGO/ZrO2 nanocomposite from aqueous solution: fixed bed column adsorption modelling and its adsorption mechanism. *Journal of Fluorine Chemistry* **194**, 40–50.

Mondal, N. K., Samanta, A., Roy, P. & Das, B. 2019 Optimization study of adsorption parameters for removal of Cr (VI) using magnolia leaf biomass by response surface methodology. *Sustainable Water Resources Management* **5** (4), 1627–1639.

Pal, D. B., Tiwari, A. K. & Giri, D. D. 2021 Various purification techniques of groundwater. In: *Groundwater Geochemistry: Pollution and Remediation Methods* (S. Madhav & P. Singh, eds.). Wiley & Sons, Hoboken, NJ, USA.

Palansooriya, K. N., Yang, Y., Tsang, Y. F., Sarkar, B., Hou, D., Cao, X., Meers, E., Rinklebe, J., Kim, K.-H. & Ok, Y. S. 2020 Occurrence of contaminants in drinking water sources and the potential of biochar for water quality improvement: a review. *Critical Reviews in Environmental Science and Technology* **50** (6), 549–611.

Patel, H. 2020 Batch and continuous fixed bed adsorption of heavy metals removal using activated charcoal from neem (Azadirachta indica) leaf powder. *Scientific Reports* **10** (1), 1–12.

Pokhrel, D. & Viraraghavan, T. 2008 Arsenic removal in an iron oxide-coated fungal biomass column: analysis of breakthrough curves. *Bioresource Technology* **99** (6), 2067–2071.

Razzak, A., Shafiquzzaman, M., Haider, H. & Alresheedi, M. 2021 Arsenic removal by iron-oxidizing bacteria in a fixed-bed coconut husk column: experimental study and numerical modeling. *Environmental Pollution* **272**, 115977.

Roy, P., Dey, U., Chattoraj, S., Mukhopadhyay, D. & Mondal, N. K. 2013 Removal of arsenic (III) and arsenic (V) on chemically modified low-cost adsorbent: batch and column operations. *Applied Water Science* **3** (1), 293–309.

Roy, P., Mondal, N. K., Bhattacharya, S., Das, B. & Das, K. 2017 Modeling of the adsorptive removal of arsenic (III) using plant biomass: a bioremedial approach. *Applied Water Science* **7** (3), 1307–1321.

Sawood, G. & Gupta, S. 2018 Arsenic remediation of the waste water using adsorbent: a review. *International Journal of Engineering, Technology, Science and Research* **5**, 1054–1070.

Sawood, G. M. & Gupta, S. 2020a Kinetic equilibrium and thermodynamic analyses of As (V) removal from aqueous solution using iron-impregnated Azadirachta indica carbon. *Applied Water Science* **10** (6), 1–18.

Sawood, G. M. & Gupta, S. 2020b Arsenate adsorption from aqueous solution using iron-loaded Azadirachta indica roots: batch and fixed-bed column study. *Desalin. Water Treat.* **203**, 292–308.

Sawood, G. M., Dixit, S., Mishra, G. & Gupta, S. 2021a Selective As (v) capture by a novel magnetic green Fe-biochar composite in a packed column: an application of central composite design. *Environmental Science: Water Research & Technology* **7** (11), 2129–2144.

Sawood, G. M., Mishra, A. & Gupta, S. 2021b Optimization of arsenate adsorption over aluminum-Impregnated Tea waste biochar using RSM–Central composite design and adsorption mechanism. *Journal of Hazardous, Toxic, and Radioactive Waste* **25** (2), 04020075.

Singh, A., Chauhan, S., Varjani, S., Pandey, A. & Bhargava, P. C. 2022 Integrated approaches to mitigate threats from emerging potentially toxic elements: a way forward for sustainable environmental management. *Environmental Research* **209**, 112844.

Tajik, S., Garkani-Nejad, Z., Mahmoudi-Moghaddam, H., Beitollahi, H. & Khabazzadeh, H. 2021 Electrochemical determination of levodopa and cabergoline by a magnetic core-Shell iron (II, III) oxide@ silica/Multiwalled carbon nanotube/Ionic liquid/2-(4-Oxo-3-Phenyl-3, 4-Dihydroquinazolinyl)-N′-Phenyl-Hydrazine carbothioamide (FSCNT/IL/2PHC) modified carbon paste electrode. *Analytical Letters* **54** (16), 2638–2654.

Tang, J., Huang, Y., Gong, Y., Lyu, H., Wang, Q. & Ma, J. 2016 Preparation of a novel graphene oxide/Fe-Mn composite and its application for aqueous Hg (II) removal. *Journal of Hazardous Materials* **316**, 151–158.

Wasay, S. A., Haron, M. J., Uchiumi, A. & Tokunaga, S. 1996 Removal of arsenite and arsenate ions from aqueous solution by basic yttrium carbonate. *Water Research* **30** (5), 1143–1148.

Weerasundara, L., Ok, Y.-S. & Bundschuh, J. 2021 Selective removal of arsenic in water: a critical review. *Environmental Pollution* **268**, 115668.

Wei, Y., Wei, S., Liu, C., Chen, T., Tang, Y., Ma, J., Yin, K. & Luo, S. 2019 Efficient removal of arsenic from groundwater using iron oxide nanoneedle array-decorated biochar fibers with high Fe utilization and fast adsorption kinetics. *Water Research* **167**, 115107.

Yassin, M. M., Biti, S., Afzal, W. & Martín, C. F. 2021 A systematic analysis of the dynamics of microwave-and conventionally-assisted swing adsorption on zeolite 13X and an activated carbon under post-combustion carbon capture conditions. *Journal of Environmental Chemical Engineering* **9** (6), 106835.

Yeo, K. F. H., Li, C., Zhang, H., Chen, J., Wang, W. & Dong, Y. 2021 Arsenic removal from contaminated water using natural adsorbents: a review. *Coatings* **11** (11), 1407.

Zhang, L., Zeng, Y. & Cheng, Z. 2016 Removal of heavy metal ions using chitosan and modified chitosan: a review. *Journal of Molecular Liquids* **214**, 175–191.

Zhou, J., Yu, X., Ding, C., Wang, Z., Zhou, Q., Pao, H. & Cai, W. 2011 Optimization of phenol degradation by candida tropicalis Z-04 using plackett-burman design and response surface methodology. *Journal of Environmental Sciences* **23** (1), 22–30.

Zhu, N., Zhang, J., Tang, J., Zhu, Y. & Wu, Y. 2018 Arsenic removal by periphytic biofilm and its application combined with biochar. *Bioresource Technology* **248**, 49–55.